**NURETH14-569** 

# DYNAMIC MODELING STRATEGY FOR FLOW REGIME TRANSITION IN GAS-LIQUID TWO-PHASE FLOWS

X. Wang<sup>1</sup>, X. Sun<sup>1</sup>, B. Doup<sup>1</sup> and H. Zhao<sup>2</sup>

<sup>1</sup> Nuclear Engineering Program, The Ohio State University, Columbus, OH 43210, USA
<sup>2</sup> Idaho National Laboratory, Idaho Falls, ID 83415, USA

#### **Abstract**

In modeling gas-liquid two-phase flows, the concept of flow regime has been widely used to characterize the global interfacial structure of the flows. Nearly all constitutive relations that provide closures to the interfacial transfers in two-phase flow models, such as the two-fluid model, are often flow regime dependent. Currently, the determination of the flow regimes is primarily based on flow regime maps or transition criteria, which were developed for steady-state, fully-developed flows and have been widely applied in nuclear reactor system safety analysis codes. As two-phase flows are dynamic in nature (fully-developed two-phase flows generally do not exist in real applications), it is of importance to model the flow regime transition dynamically to be able to predict two-phase flows more accurately.

The present work aims to develop a dynamic modeling strategy to determine flow regimes in gas-liquid two-phase flows through introduction of interfacial area transport equations (IATEs) within the framework of a two-fluid model. The IATE is a transport equation that models the interfacial area concentration by considering the creation and destruction of the interfacial area, such as the fluid particle (bubble or liquid droplet) disintegration, boiling and evaporation; and fluid particle coalescence and condensation, respectively. For the flow regimes beyond bubbly flows, a two-group IATE has been proposed, in which bubbles are divided into two groups based on their size and shapes, namely group-1 and group-2 bubbles. A preliminary approach to dynamically identify the flow regimes is discussed, in which discriminators are based on the predicted information, such as the void fraction and interfacial area concentration. The flow regime predicted with this method shows good agreement with the experimental observations.

#### 1. Introduction

Gas-liquid two-phase flows are common in nuclear reactor systems, such as those during steady-state operation and transients in light water reactors (LWRs). It is observed that two-phase flows under various flow and operating conditions show significantly different interfacial structure characteristics as well as flow behaviors, such as interfacial mass and heat transfer, drag force, wall heat transfer. The concept of flow regime/pattern was introduced to better understand and model different flows [1-3]. Flow regime maps or transition criteria, developed from experiments carried out for steady-state, fully developed flows, are widely used to determine flow regimes [1-3]. This static method presents inherent shortcomings as two-phase flows are dynamic in nature (fully-developed two-phase flows generally do not exist in real applications). In addition, this approach assumes that one flow regime can potentially be switched to a different flow regime instantaneously without considering any time scale or length scale,

provided that the flow regime transition criteria are met. In reality, the occurrence of the flow regime transition is not instantaneous, and it requires time (and therefore length) for the flow to develop.

In two-phase flow simulations, interfacial transfer terms need to be modeled to provide closures to two-phase flow models, specially the two-fluid model. An interfacial transfer term can generally be modeled as the product of the interfacial area concentration (IAC), a geometric parameter characterizing the interfacial transfer "capability," and the corresponding driving potential [4]. In most nuclear reactor system safety analysis codes, such as RELAP5, the modeling of interfacial transfers is a two-step approach [5]: first to identify the flow regime of the two-phase flow based on the available information using the aforementioned flow regime maps or transition criteria, and secondly, to obtain the constitutive relations of the interfacial transfers for the corresponding flow regime. Errors will be produced in each step, and compound errors from these two steps may not be trivial.

As argued by Ishii et al. [6], among others, many of the current system analysis codes have been extensively benchmarked against relevant separate-effects and integral tests. As a result, the integral response of the interfacial transfers is typically reasonably captured by the codes, but the compensating errors in these interfacial transfer models could have been introduced. As an example, RELAP5 is usually capable of predicting an event progress following an initiating event, given that the scenario is within the range of the code validity. A very complicated flow regime map with straight transition lines/or flat transition surfaces is employed in RELAP5 [7]. These flow regime maps are applied to both developing and transient flows. Due to the static nature of the flow regime maps, the modeling approach of the constitutive relations is therefore static. This discrepancy between the actual flow dynamics and the static modeling of the interfacial transfers represents potentially significant shortcomings [8, 9], and should be improved upon for next generation advanced system safety analysis codes, which are expected to "get the right answer for the right reasons" in the analysis of the current and advanced future passive LWRs. In view of this, Kelly [8] proposed to dynamically model the spatial evolution of two-phase flow regimes through the introduction of interfacial area transport equation (IATE).

In the present work, a dynamic modeling strategy for determining flow regimes in gas-liquid two-phase flows has been developed within the framework of the two-fluid model coupled with the IATE model. In this approach, the IAC is evaluated by the IATE model that accounts for both the fluid particle (bubble or liquid droplet) interaction mechanisms and phase changes [10-13]. The interfacial transfer terms can therefore be constructed without the predetermination of the flow configurations using flow regime maps. In addition, the method to identify various flow regimes is proposed, in which discriminators are based on the predicted flow information, such as the void fraction and IAC. This method is expected to, if applied to computer codes, improve their predictive capabilities of gas-liquid two-phase flows, in particular for the applications in which flow regime transition occurs.

# 2. Theory and Modeling Strategy

### 2.1 Two-group IATE

Bubbles of gas-liquid two-phase flows can be categorized into spherical, distorted, cap, Taylor (slug), and churn-turbulent bubbles, associated with different flow behaviors, e.g., the relative motion and bubble interaction mechanisms [12-14]. In the current study, bubbles are separated into two distinct

groups, with the maximum distorted bubble size limit  $D_{d,\max}$  as the group boundary. The group-1 bubbles consisting of spherical and distorted bubbles exist in the range from minimum bubble size to  $D_{d,\max}$ ; whereas the group-2 bubbles consisting of cap, Taylor (slug), and churn-turbulent bubbles exist in the range from  $D_{d,\max}$  to maximum stable bubble size limit  $D_{c,\max}$ . These bubble size boundaries were given by Ishii and Zuber [15] as:

$$D_{d,\text{max}} = 4\sqrt{\sigma/(g\Delta\rho)} \text{ and } D_{c,\text{max}} = 40\sqrt{\sigma/(g\Delta\rho)},$$
 (1)

where,  $\sigma$ : surface tension,  $\Delta \rho$ : density difference between the two phases, g: gravitation acceleration.

The two-group IATE model has been developed to model the IAC for each group of bubbles in general two-phase flows. The transport equations in the two-group IATE model are obtained by averaging the Boltzmann transport equation of bubble surface area per mixture volume over the volume range of each bubble group and formulated as [12, 13]:

$$\frac{\partial a_{i1}}{\partial t} + \nabla \cdot \left(a_{i1}\vec{v}_{i1}\right) = \frac{a_{i1}}{\alpha_{g1}} \left[ \frac{2}{3} - \chi \left( \frac{D_{sc}}{D_{sm1}} \right)^{2} \right] \left\{ \frac{\partial \alpha_{g1}}{\partial t} + \nabla \cdot \left(\alpha_{g1}\vec{v}_{g1}\right) - \eta_{ph} \right\} + \int_{V_{\min}}^{V_{c}} \left( \sum_{j} S_{j} + S_{ph} \right) A_{i} dV, \tag{2}$$

$$\begin{split} \frac{\partial a_{i2}}{\partial t} + \nabla \cdot \left( a_{i2} \vec{v}_{i2} \right) &= \frac{2}{3} \frac{a_{i2}}{\alpha_{g2}} \left\{ \frac{\partial \alpha_{g2}}{\partial t} + \nabla \cdot \left( \alpha_{g2} \vec{v}_{g2} \right) \right\} \\ &+ \chi \left( \frac{D_{sc}}{D_{sm1}} \right)^{2} \frac{a_{i1}}{\alpha_{g1}} \left\{ \frac{\partial \alpha_{g1}}{\partial t} + \nabla \cdot \left( \alpha_{g1} \vec{v}_{g1} \right) - \eta_{ph} \right\} + \int_{V_{c}}^{V_{\text{max}}} \sum_{j} S_{j} A_{i} dV, \end{split} \tag{3}$$

where, subscripts g, 1, and 2: gas phase, group-1, and group-2 bubbles, respectively,  $a_i$ : interfacial area concentration,  $\vec{v}_i$ : interfacial velocity,  $\alpha$ : void fraction, t: time,  $\vec{v}$ : velocity,  $\eta_{ph}$ : rate of volume generated by nucleation source per unit mixture volume,  $\chi$ : coefficient accounting for the contribution from the inter-group transfer,  $V_{\min}$ ,  $V_c$  and  $V_{\max}$ : volumes of minimum bubble, critical bubble and maximum bubble, respectively,  $D_{sc}$ : surface equivalent diameter of a fluid particle with critical volume  $V_c$ ,  $D_{sm}$ : Sauter mean diameter defined as  $6\alpha/a_i$ ,  $S_j$  and  $S_{ph}$ : particle source and sink rate per unit mixture volume due to the j-th particle interaction (coalescence and disintegration) and that due to phase change, respectively. The two-group IATE can be simplified to a one-group IATE applicable to bubbly flow regime. In the literature, bubble interaction terms have been modeled extensively [10-13] while the phase change effects warrants further studies [16, 17].

#### 2.2 The three-field two-fluid model

To incorporate the two-group IATE model to a two-fluid model, the modified three-field two-fluid model proposed by Sun et al. [18] is used. In this modified model, mass transfer occurs not only between

the gas and liquid phases due to phase change, but also between group-1 and group-2 bubbles due to intra- and inter-group bubble interactions. Three fields are defined, namely, group-1 bubbles as field-1, group-2 bubbles as field-2, and the liquid phase as field-3. Two sets of conservation equations are used for the gas phase, one set for each of the two bubble groups. The pressure and temperature for group-1 and group-2 bubbles are assumed to be approximately the same in general while the velocities of two groups of bubbles differ. In what follows, the governing equations (continuity, momentum, and energy) are provided [18].

## Continuity equations:

$$\frac{\partial \left(\alpha_{g1}\rho_{g}\right)}{\partial t} + \nabla \cdot \left(\alpha_{g1}\rho_{g}\vec{v}_{g1}\right) = \Gamma_{g1} - \Delta \dot{m}_{12},\tag{4}$$

$$\frac{\partial \left(\alpha_{g2}\rho_{g}\right)}{\partial t} + \nabla \cdot \left(\alpha_{g2}\rho_{g}\vec{v}_{g2}\right) = \Gamma_{g2} + \Delta \dot{m}_{12}, \tag{5}$$

$$\frac{\partial(\alpha_f \rho_f)}{\partial t} + \nabla \cdot (\alpha_f \rho_f \vec{v}_f) = \Gamma_f, \tag{6}$$

where, subscript f: liquid phase,  $\rho$ : density,  $\Gamma$ : mass generation due to phase change,  $\Delta \dot{m}_{12}$ : intergroup mass transfer due to hydrodynamic mechanisms.

### Momentum equations:

$$\begin{split} \frac{\partial \left(\alpha_{g1}\rho_{g}\vec{v}_{g1}\right)}{\partial t} + \nabla \cdot \left(\alpha_{g1}\rho_{g}\vec{v}_{g1}\vec{v}_{g1}\right) &= -\alpha_{g1}\nabla p_{g1} + \nabla \cdot \left[\alpha_{1}\left(\overline{\overline{\tau}}_{g1}^{\mu} + \overline{\overline{\tau}}_{g1}^{T}\right)\right] \\ &+ \alpha_{g1}\rho_{g}\vec{g} + \left(\Gamma_{g1} - \Delta \dot{m}_{12}\right)\vec{v}_{gi1} - \nabla \alpha_{1} \cdot \overline{\overline{\tau}}_{gi1} + \vec{M}_{g1} + \left(p_{gi1} - p_{g1}\right)\nabla \alpha_{g1}, \end{split} \tag{7}$$

$$\begin{split} \frac{\partial \left(\alpha_{g2}\rho_{g}\vec{v}_{g2}\right)}{\partial t} + \nabla \cdot \left(\alpha_{g2}\rho_{g}\vec{v}_{g2}\vec{v}_{g2}\right) &= -\alpha_{2}\nabla p_{g2} + \nabla \cdot \left[\alpha_{2}\left(\overline{\overline{\tau}}_{g2}^{\mu} + \overline{\overline{\tau}}_{g2}^{T}\right)\right] \\ &+ \alpha_{g2}\rho_{g}\vec{g} + \left(\Gamma_{g2} + \Delta \dot{m}_{12}\right)\vec{v}_{g2} - \nabla \alpha_{2} \cdot \overline{\overline{\tau}}_{g2} + \vec{M}_{g2} + \left(p_{g2} - p_{g2}\right)\nabla \alpha_{g2}, \end{split} \tag{8}$$

$$\begin{split} \frac{\partial(\alpha_{f}\rho_{f}\vec{v}_{f})}{\partial t} + \nabla \cdot (\alpha_{f}\rho_{f}\vec{v}_{f}\vec{v}_{f}) &= -\alpha_{f}\nabla p_{f} + \nabla \cdot \left[\alpha_{f}(\overline{\overline{\tau}}_{f}^{\mu} + \overline{\overline{\tau}}_{f}^{T})\right] \\ &+ \alpha_{f}\rho_{f}\vec{g} - \nabla \alpha_{f} \cdot \overline{\overline{\tau}}_{fi} + \vec{M}_{f} + \left(p_{fi} - p_{f}\right)\nabla \alpha_{f}, \end{split} \tag{9}$$

where, subscript i: interfacial, p: pressure,  $\bar{\tau}^{\mu}$ : viscous stress,  $\bar{\tau}^{T}$ : turbulent stress,  $\bar{M}$ : generalized interfacial drag force.

## Energy equations:

$$\begin{split} \frac{\partial(\alpha_{\scriptscriptstyle 1}\rho_{\scriptscriptstyle g}H_{\scriptscriptstyle g1})}{\partial t} + \nabla \cdot (\alpha_{\scriptscriptstyle 1}\rho_{\scriptscriptstyle g}\vec{v}_{\scriptscriptstyle g1}H_{\scriptscriptstyle g1}) &= -\nabla \cdot \left(\alpha_{\scriptscriptstyle 1}\vec{q}_{\scriptscriptstyle g1}^{\prime\prime}\right) + \frac{D_{\scriptscriptstyle g}(\alpha_{\scriptscriptstyle 1}p_{\scriptscriptstyle g1})}{Dt} + a_{\scriptscriptstyle i1}q_{\scriptscriptstyle gi1}^{\prime\prime} \\ &+ (\Gamma_{\scriptscriptstyle g1} - \Delta \dot{m}_{\scriptscriptstyle 12})H_{\scriptscriptstyle gi1} - p_{\scriptscriptstyle gi1}\frac{D_{\scriptscriptstyle g}\alpha_{\scriptscriptstyle 1}}{Dt} + \phi_{\scriptscriptstyle g1}, \end{split} \tag{10}$$

$$\begin{split} \frac{\partial(\alpha_{2}\rho_{g}H_{g2})}{\partial t} + \nabla \cdot (\alpha_{2}\rho_{g}\vec{v}_{g2}H_{g2}) &= -\nabla \cdot \left(\alpha_{2}\vec{q}_{g2}''\right) + \frac{D_{g}(\alpha_{2}p_{g2})}{Dt} + a_{i2}q_{gi2}''\\ &+ (\Gamma_{g,2} + \Delta \dot{m}_{12})H_{gi2} - p_{gi2}\frac{D_{g}\alpha_{2}}{Dt} + \phi_{g2}, \end{split} \tag{11}$$

$$\begin{split} \frac{\partial(\alpha_{f}\rho_{f}H_{f})}{\partial t} + \nabla \cdot (\alpha_{f}\rho_{f}\vec{v}_{f}H_{f}) &= -\nabla \cdot \left(\alpha_{f}\vec{q}_{f}''\right) + \frac{D_{g}(\alpha_{f}p_{f})}{Dt} + a_{it}q_{fi}'' \\ &+ \Gamma_{f}H_{fi} - p_{fi}\frac{D_{g}\alpha_{f}}{Dt} + \phi_{f}, \end{split} \tag{12}$$

where, H: enthalpy,  $\vec{q}''$ : heat flux,  $q_i''$ : interfacial heat flux,  $\phi$ : dissipation.

# 2.3 Flow regime identification

Once the three-field two-fluid model is solved together with the two-group IATE, the information of the void fraction, IAC, bubble velocities of group-1 and group-2 bubbles in addition to others, will be available. Figure 1 shows a flowchart representing a proposed process of utilizing the available information to determine the flow regime for a certain flow condition.

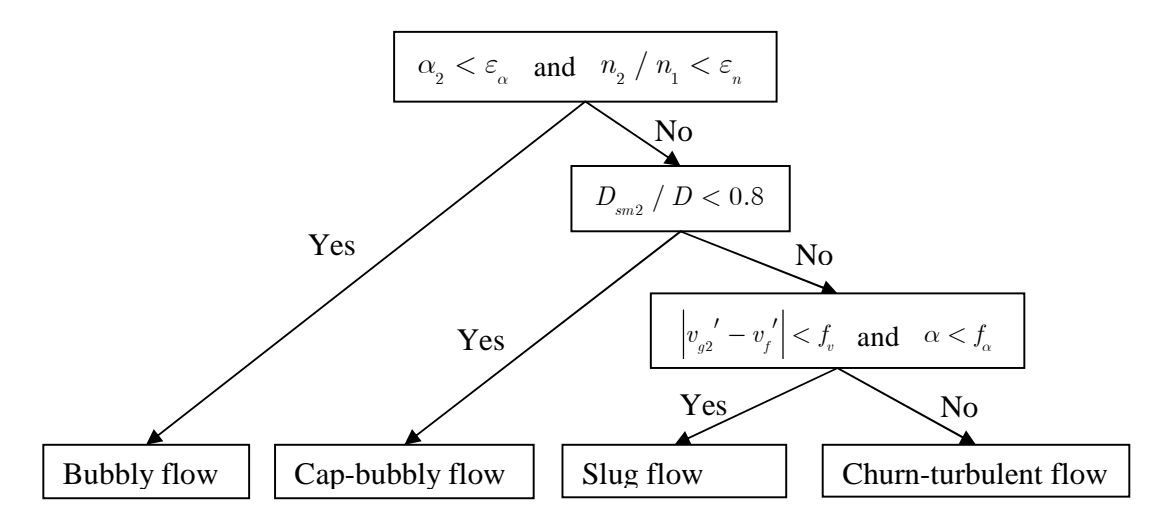


Figure 1 Flowchart for determining the flow regimes.

The identification of bubbly flow regime is relatively easy. The transition from bubbly flow to cap-bubbly (or cap-turbulent) flow is characterized by the appearance of cap bubbles in the flow, which leads to a non-zero void fraction of group-2 bubbles. In numerical analyses, a considerably small value  $\varepsilon_{\alpha}$  is

used instead of zero due to machine errors. In addition, the bubble number density is also used as the second criterion, which is defined for each of the bubble group as:

$$n_1 = \frac{a_{i1}^3}{36\pi\alpha_1^2}$$
 and  $n_2 = \frac{a_{i2}^3}{36\pi\alpha_2^2}$ . (13)

At the bubbly to cap-bubbly transition, the ratio of the bubble number densities of group-2 to group-1 bubbles, i.e.,  $n_2/n_1$ , increases significantly from zero.

The determination of cap-bubbly flows in a circular pipe may be based on the bubble Sauter mean diameter  $D_{sm}$ . Figure 2 shows a schematic of a Taylor (slug) bubble, which has a spherical nose at its front plus a cylindrical gas volume with a diameter  $\eta D$ . D is the inner diameter of the pipe. The wake angle of the leading spherical nose,  $2\theta$ , can be approximated as 100 degree [19]. For a perfect cap bubble, the cylindrical gas volume diminishes, so its length in the flow direction L is reduced to  $\frac{\eta D}{2\sin\theta}(1-\cos\theta)$ . The Sauter mean diameter of this cap bubble, plotted in Fig. 3, can be therefore calculated based on its volume and surface area.

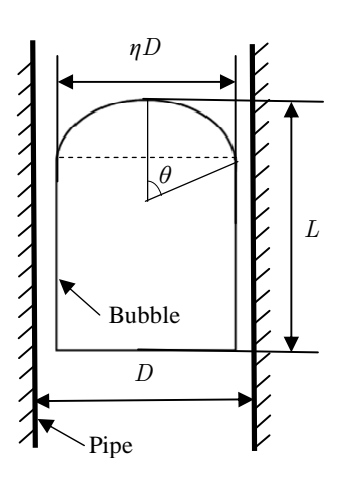


Figure 2 A schematic of a Taylor bubble of length L and diameter  $\eta D$  in a pipe of inner diameter D.

Similarly the Sauter mean diameter of a slug bubble shown in Fig. 2 can be obtained provided that the length of the slug bubble is known. Since the transition from cap-bubbly flow to slug flow is of interest, the slug bubble size near the transition region is examined. According to Govier and Aziz [20], the transition is considered to have occurred from cap-bubbly to slug flows once the chord length of the elongated "cap" bubble shown in Fig. 2 reaches the pipe inner diameter, i.e., when L=D. Adopting this assumption, the Sauter mean diameter for this type slug bubbles can be computed and is plotted in Fig. 3 as "Taylor bubble." Since the diameter of a stable Taylor bubble usually exceeds ¾ of the pipe inner diameter [20], the Sauter mean diameter for Taylor bubbles is only plotted for  $\eta \ge 0.75$ . From this plot, it is clear that the Sauter mean diameter of group-2 bubbles can be quite distinct for ideal cap

bubbles and Taylor bubbles. In addition, an increase in the chord length of a Taylor bubble would increase the value of  $D_{\rm sm2}$  / D.

Furthermore, investigations over the experimental data indicates an increase in  $D_{\scriptscriptstyle sm2}$  for churn-turbulent bubbles compared to more structured slug bubbles, perhaps because of the inherent chaotic feature and irregular shape of the churn-turbulent bubbles. Therefore, flow will be identified as capbubbly flow once the value of  $D_{\scriptscriptstyle sm2}$  / D is less than 0.8.

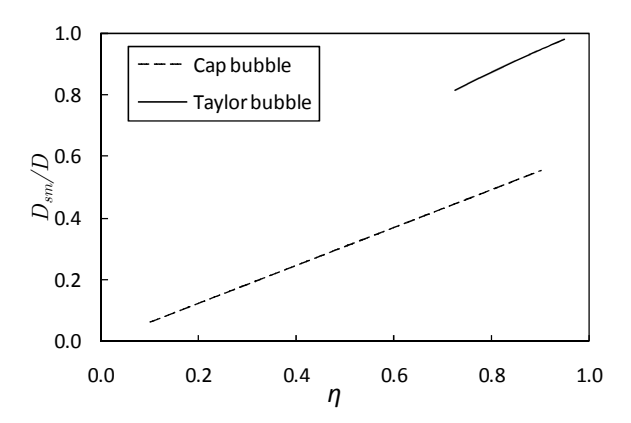


Figure 3 Ratio of the Sauter mean diameters of a cap and slug bubble (at its initiating stage) to the pipe diameter as a function of the bubble size ( $\eta D$ ).

The next task is to distinguish the slug flow from churn-turbulent flow, which is most challenging. Churn-turbulent flow is chaotic and involves significant flow churning and perhaps local re-circulation. Two preliminary discriminators are proposed here, namely, the absolute value of the velocity difference between group-2 bubbles and the continuous liquid phase  $(\left|v_{g^2}\right| - \left|v_f\right|)$  and the total void fraction.

The first discriminator is based on the work conducted by Van der Geld [21]. He studied the onset of churn flows theoretically and concluded that the flow turns into churn flow if it follows

$$\left|v_{g2}' - v_f'\right| > f_v,$$
 (14)

where,  $v_{g2}'$ : gas velocity at the tube center,  $v_f'$ : mean velocity of the water film.  $f_v$  is a function of flow variables and tube geometry, and was provided as [21]:

$$f_{v} = 0.281 \left(50D\right)^{1.322} \exp\left(0.044T\right) \left(10^{4}h\right)^{s} \sqrt{\frac{\sigma}{\rho_{g}} \frac{1}{\left(0.5D - h\right)}},\tag{15}$$

where,  $s=-\left(50D\right)^{-0.147}\left(0.5946+0.00728T\right)$ , T: temperature in  ${}^{\rm o}{\rm C}$ , h: water film thickness. However, it is difficult to evaluate  $f_v$  since the estimation of the water film thickness in numerical calculations and experimental studies remains a question to be answered.

The second discriminator is more practical, which was proposed by Mishima and Ishii [3] using the void fraction. They pointed out that it becomes churn-turbulent flow once the tail of the preceding slug bubble starts to touch the nose of the following bubble and derived the slug-to-churn flow transition criterion. Their criterion is adopted and modified with the assumption that the thickness of the liquid film near the wall region is about 5% of the pipe diameter, given as:

$$\alpha \ge f_{\alpha}$$
. (16)

Here,  $f_{\alpha}$  is given as:

$$f_{\alpha} = 0.81 \left\{ 1 - 0.813 \left[ \frac{\left( C_0 - 1 \right) \left( j_g + j_f \right) + 0.35 \sqrt{\Delta \rho g D / \rho_f}}{\left( j_g + j_f \right) + 0.75 \sqrt{\Delta \rho g D / \rho_f} \left( \Delta \rho g D^3 / \rho_f \nu_f^2 \right)^{1/18}} \right]^{0.75} \right\}, \tag{17}$$

where,  $C_0$ : distribution parameter, j: superficial velocity,  $\nu$ : kinematic viscosity.

#### 3. Experimental Study

An experimental study on the flow regime transition in a vertical air-water test loop was performed to examine the proposed flow regime transition criteria. The test facility has the following operating capability: water temperature range of 20-90 °C, air temperature of 20 °C, and system pressure of approximately 1 bar. A schematic of the test facility is shown in Fig. 4.

The test section in the loop is a circular pipe with an inner diameter of 50 mm (2 inch) and a height of 2.8 m. The main component of the bubble injector is a sintered metal sparger with an average pore size of 40 microns. Compressed air passes through this sparger and air bubbles form on the outer surface. These air bubbles are then dislodged from the sparger surface by an auxiliary water supply that flows through the annulus formed by the sparger and the outer pipe of the bubble injector. The maximum achievable air and water superficial velocities are 5.7 and 2.0 m/s, respectively. The initial bubble size can be varied by adjusting the flow distribution between the flow that enters the manifold before entering the test section (main water flow) and the auxiliary water flow. Controlling this flow distribution allows for direct control of the water velocity that shears the bubbles from the sparger surface thereby controlling the size of the bubbles that are entrained in the water flow.

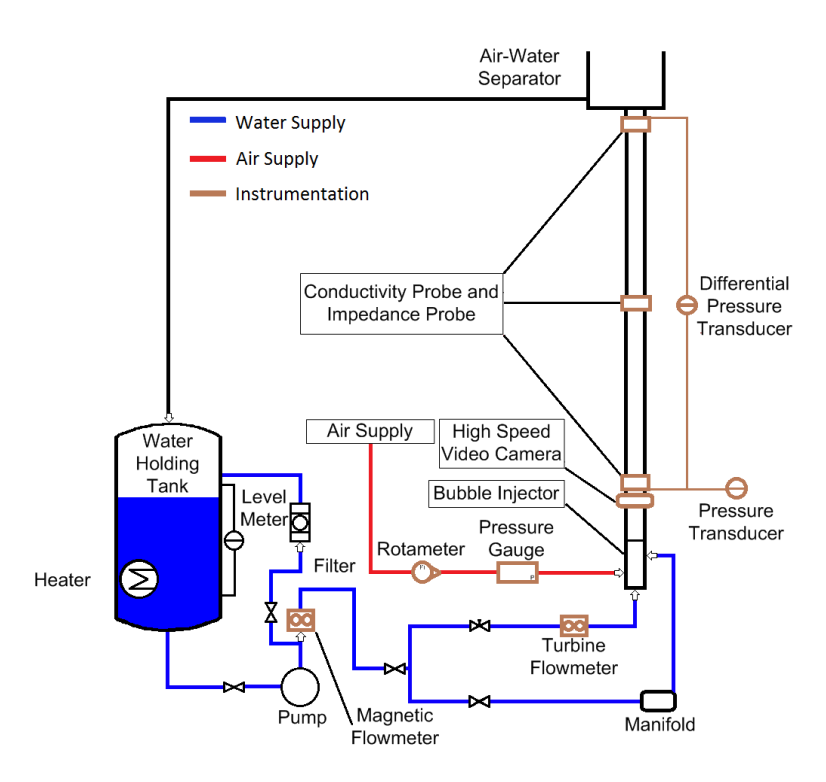


Figure 4 Schematic of the air-water test facility.

The instruments used to observe the two-phase flow characteristics are a high-speed video camera, a differential pressure transducer, impedances probes [22, 23], and four-sensor conductivity probes [24]. The high-speed video camera is capable of recording 32,000 frames per second and has a maximum shutter speed of 1/272,000 s, and is employed to visualize the flow and capture flow images to help analyze different flow conditions. The differential pressure transducer, impedance probes, and four-sensor conductivity probe are used to measure the flow parameters, such as the pressure drop, and bubble size, void fraction, bubble velocity, and IAC for group-1 and group-2 bubbles. The impedance probes and four-sensor conductivity probes are installed at axial locations 10, 32, and 54 pipe diameters above the bubble injector.

#### 4. Model Benchmark

Experiments were performed under different flow conditions, among which six cases are discussed here. Figure 5 illustrates the images captured by the high-video camera for typical bubbly, cap-bubbly, slug, and churn-turbulent flows, respectively.

Table 1 provides the area-averaged values of local flow parameters and other calculated parameters of interest in each flow condition. z is the axial location above the bubble injector. The flow regime of each flow condition determined from the visualization and the captured images is shown in the "Experimental visualization" column in Table 1 and also plotted in Fig. 6. In Table 1, flows at lower measured location with high flow rates (Runs 4, 5, and 6) include relatively large cap bubbles with strong turbulence possibly due to the bubble injectors. Therefore, we categorize those flows as cap-turbulent flows. In Fig.

6, " $\square$ ,  $\triangle$ , O,  $\diamondsuit$ " represents the bubbly, cap (either cap-bubbly or cap-turbulent), slug, and churn flows observed in the experiments. Unfilled symbols represent the measurements at lower location, i.e., at z = 0.5 m, and solid symbols represents the measurements at higher locations, i.e., at z = 1.6 m in Runs 2 and 3, and at z = 2.7 m in Runs 4, 5, and 6, respectively. It is noted that cap-bubbly flow was not identified by Mishima and Ishii [3] and some of our observations disagree with their approach. This may be due to the length needed for the flow to develop.

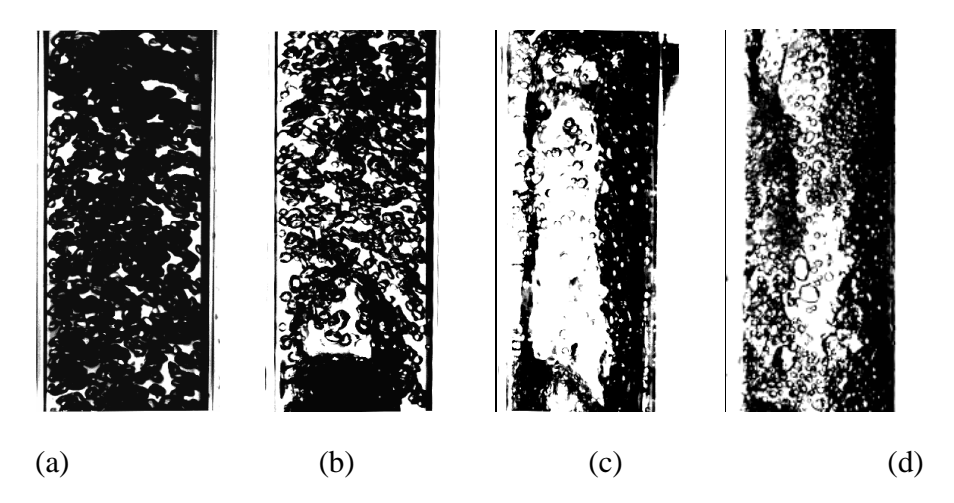


Figure 5 Flow images captured by the high video camera: (a) bubbly, (b) cap-bubbly, (c) slug, and churn-turbulent flows.

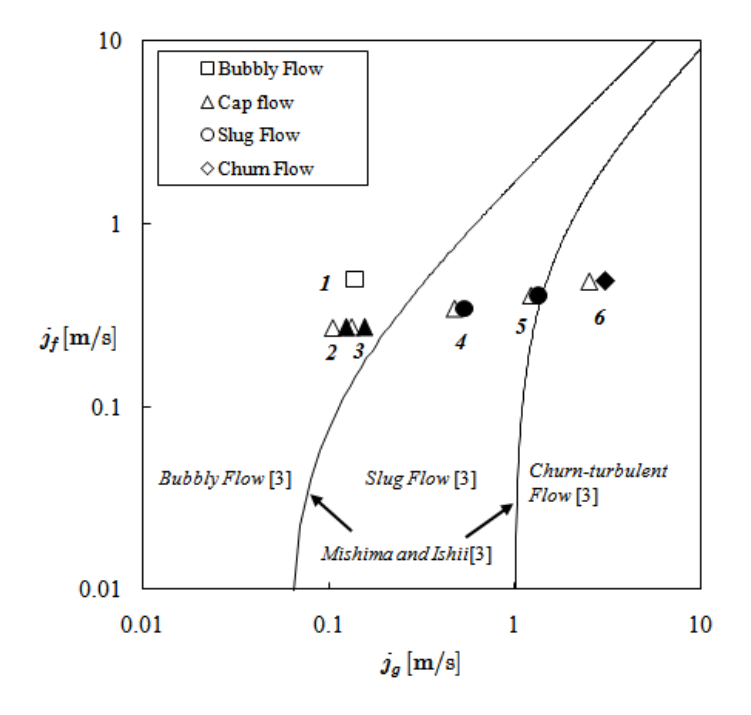


Figure 6 Flow conditions in flow regime map [3].

The 14<sup>th</sup> International Topical Meeting on Nuclear Reactor Thermalhydraulics, NURETH-14 Toronto, Ontario, Canada, September 25-30, 2011

Table 1 Measured and calculated flow parameters from experiments

Run #	z (m)	$j_g$ (m/s)	$j_f$ (m/s)	$\alpha_1$	$\alpha_{_{2}}$	α	$n_2/n_1^{-1}$	$D_{sm2}$ / $D^2$	$v_{g1}$ - $v_f$ (m/s)	$v_{g2}$ - $v_f$ (m/s)	$f_{\alpha}^{3}$	Experimental visualization	Determined by flowchart in Fig. 1
1	0.5	0.14	0.50	0.079	0	0.079	0	0	-0.20	=	0.65	Bubbly	Bubbly
2	0.5	0.11	0.27	0.15	0.034	0.17	0.058	0.17	0.71	0.74	0.65	Cap-bubbly	Cap
	1.6	0.12	0.27	0.15	0.028	0.18	0.024	0.21	0.28	0.27	0.65	Cap-bubbly	Cap
3	0.5	0.13	0.27	0.075	0.13	0.20	0.22	0.21	1.19	1.11	0.65	Cap-bubbly	Cap
	1.6	0.15	0.27	0.082	0.12	0.20	0.083	0.39	0.37	0.35	0.65	Cap-bubbly	Cap
4	0.5	0.48	0.34	0.060	0.36	0.42	0.30	0.41	1.94	1.88	0.64	Cap-turbulent	Cap
	2.7	0.53	0.34	0.12	0.28	0.40	0.071	0.84	0.58	0.51	0.64	Slug	Slug
5	0.5	1.22	0.40	0.048	0.45	0.51	0.44	0.46	2.37	2.45	0.64	Cap-turbulent	Cap
	2.7	1.33	0.40	0.11	0.44	0.55	0.081	1.29	0.82	0.70	0.64	Slug	Slug
6	0.5	2.52	0.48	0.036	0.52	0.57	0.79	0.60	3.25	4.78	0.63	Cap-turbulent	Cap
	2.7	3.05	0.48	0.087	0.56	0.65	0.23	0.88	1.56	1.31	0.63	Churn	Churn

 $<sup>^{1}</sup>$ :  $n_{2}/n_{1}$  was calculated based on the measured bubble number densities of group-1 and group-2 bubbles.

 $<sup>^{2}\!\!:\;</sup>D_{{\it sm2}}\;$  was calculated based on the measured void fraction and IAC.

 $<sup>^3</sup>$ :  $f_{\alpha}$  was calculated based on the measured data.

Therefore, it is more reasonable to determine the flow regime using a dynamic approach, e.g., the algorithm proposed in the current work. Following the flowchart provided in Fig. 1, the flow regime is determined and provided in the "Determined by flowchart in Fig. 1" column in Table 1. Take the flow at z=2.7 m in Run 6 as an example. First of all, since the values of  $\alpha_2$  and  $n_2/n_1$  are relatively large, it is not bubbly flow. Secondly, the value of  $D_{sm2}/D$  is larger than 0.8, the flow should be either slug or churn flow, i.e., it is not cap-bubbly flow. Finally, since the total void fraction is slightly greater than  $f_{\alpha}$ , which is calculated to be 0.63 in this case, the flow at z=2.7 m in Run 6 is identified as churn-turbulent flow. Good agreement has been achieved between the experimental visualizations and our results shown in Table 1.

#### 5. Conclusions

In summary, a dynamic modeling approach for the two-phase flow regimes was proposed and limited comparisons were carried out based on the air-water two-phase flow experiments performed in the current work. Compared to the static approach proposed in the literature, this dynamic approach shows good agreement and is more consistent with the two-fluid model. This method will be helpful to develop a next generation, multi-physics reactor system analysis code for the safety and performance analysis of existing and future light water reactor systems with high fidelity. It is necessary however to further validate the proposed model with more experimental data. In addition, it is planned to implement the modified two-fluid model and two-group IATE into codes and benchmark the transition models against the separate-effects experimental data obtained in this study as well as others available.

## 6. References

- [1] M. Ishii and K. Mishima, "Study of two-fluid model and interfacial area," ANL-80-111, Argonne National Laboratory Report, 1980.
- [2] Y. Taitel, D. Bornea, and A.E. Dukler, "Modeling flow pattern transitions for steady upward gas-liquid flow in vertical tubes," *AICHE Journal*, Vol. 26, No. 3, 1980, pp. 345-354.
- [3] K. Mishima and M. Ishii, "Flow regime transition criteria for upward two-phase flow in vertical tubes," *Int. J. Heat Mass Transfer*, Vol. 27, No. 5, 1984, pp. 723-737.
- [4] H. Städtke, "Thermal-hydraulic codes for LWR safety analysis present status and future perspective," NUREG/CP-0159, U.S. Nuclear Regulatory Commission, 1996, pp. 732-750.
- [5] T. Hibiki and M. Ishii, "Two-group interfacial area transport equations at bubbly-to-slug flow transition," *Nuc. Eng. Des.*, Vol. 202, 2000, pp. 39-76.
- [6] M. Ishii, S. Kim, and J. Uhle, "Interfacial area transport: data and models," NEA/CSNI/R(2001)2, Nuclear Energy Agency, Paris, 2000, pp. 517-538.
- [7] The RELAP5-3D Code Development Team, "RELAP5-3D code manual volume IV: models and correlations," INEEL-EXT-98-00834, Revision 2.4, Idaho National Laboratory, June 2005, pp. 3-9.

- [8] J.M. Kelly, "Constitutive model development needs for reactor safety thermal-hydraulic codes," NUREG/CP-0160, U.S. Nuclear Regulatory Commission, 1997, pp. 3-29.
- [9] H. Städtke, Gas-dynamic Aspects of Two-phase Flow: Hyperbolocity, Wave Propagation, Phenomena, and Related Numerical Methods, Wiley-VCH, 2006.
- [10] G. Kocamustafaogullari and M. Ishii, "Foundation of the interfacial area transport equation and its closure relation," *Int. J. Heat Mass Transfer*, Vol. 38, 1995, pp. 481-493.
- [11] Q. Wu, S. Kim, M. Ishii, and S.G. Beus, "One-group interfacial area transport in vertical bubbly flow," *Int. J. Heat Mass Transfer*, Vol. 41, No. 8-9, 1998, pp. 1103-1112.
- [12] X. Fu and M. Ishii, "Two-group interfacial area transport in vertical air-water flow: I. mechanistic model," *Nucl. Eng. Des.*, Vol. 219, 2003, pp. 143-168.
- [13] X. Sun, S. Kim, M. Ishii, and S.G. Beus, 2004, "Modeling of bubble coalescence and disintegration in confined upward two-phase flow," *Nucl. Eng. Des.*, Vol. 230, pp. 3-26.
- [14] M. Ishii and T. Hibiki, *Thermo-fluid Dynamics of Two-Phase Flow*, Springer, 2006.
- [15] M. Ishii and N. Zuber, "Drag coefficient and relative velocity in bubbly, droplet or particulate flows," *AICHE Journal*, Vol. 25, 1979, pp. 843-855.
- [16] R. Situ, M. Ishii, T. Hibiki, J.Y. Tu, G.H. Yeoh, and M. Mori, "Bubble departure frequency in forced convective subcooled boiling flow," *Int. J. Heat Mass Transfer*, Vol. 51, 2008, pp. 6268-6282.
- [17] H.S. Park, T.H. Lee, T. Hibiki, W.P. Baek, and M. Ishii, "Modeling of the condensation sink term in an interfacial area transport equation," *Int. J. Heat Mass Transfer*, Vol. 50, 2007, pp. 5041-5053.
- [18] X. Sun, M., Ishii, and J.M. Kelly, "Modified two-fluid model for the two-group interfacial area transport equation," *Ann. Nucl. Energy*, Vol. 30, 2003, pp. 1601-1622.
- [19] R. Clift, J.R. Grace, and M.E. Weber, *Bubbles, Drops, and Particles*, Academic Press, Inc, 1978.
- [20] G.W. Govier and K. Aziz, *The Flow of Complex Mixtures in Pipes*, Van Nostrand Reinhold Co., New York, 1972, pp. 388-389.
- [21] C.W.M. van der Geld, "The onset of churn flow in vertical tubes: effects of temperature and tube radius," Report WOP-WET 85.010, Technische Hogeschool Eindhoven, Netherlands, 1985.
- [22] X. Sun, S. Kuran, and M. Ishii, "Cap bubbly-to-slug flow regime transition in a vertical annulus," *Experiments in Fluids*, Vol. 37, No. 3, 2004, pp. 458-464.
- [23] Y. Mi, "Two-phase flow characterization based on advanced instrumentation, neural networks, and mathematical modeling," Ph.D. Thesis, Purdue University, West Lafayette, IN, 1998.
- [24] S. Kim, X.Y. Fu, X. Wang, and M. Ishii, "Development of the miniaturized four sensor conductivity probe and the signal processing scheme," *Int. J. Heat Mass Transfer*, Vol. 43, No. 22, 2000, pp. 4101-4118.